The Astrophysical Journal, 850:57 (11pp), 2017 November 20 https://doi.org/10.3847/1538-4357/aa9078

Plasma Measurements of the Fe XVII L-shell Emission and Blending with F VIII and F IX

P. Beiersdorfer[1], J. K. Lepson[2], M. F. Gu[2], and M. Bitter[3]
[1] Lawrence Livermore National Laboratory, Physics Division, Livermore, CA 94551, USA
[2] University of California Berkeley, Space Sciences Laboratory, Berkeley, CA 94720, USA
[3] Princeton University, Princeton Plasma Physics Laboratory, Princeton, NJ 08543, USA
Received 2017 June 12; revised 2017 September 20; accepted 2017 September 28; published 2017 November 16

Abstract

We measured the L-shell emission spectrum of Fe XVII in a low-density, low-gradient magnetically confined laboratory plasma that contains predominately C, O, Fe, and Ni as trace elements and found excellent agreement with the relative spectral emission obtained in solar and astrophysical observations. However, we obtained spectra that appear to have an usually large $1s^22s^22p_{1/2}^5 3d_{3/2} \rightarrow 1s^22s^22p^6$ Fe XVII resonance transition, which is commonly labeled $3C$, from hot plasmas that also contain fluorine. The wavelength of the Lyα feature of F IX is coincident with the wavelength of the Fe XVII line $3C$ within one part in 538, and its flux, therefore, enhances the Fe XVII resonance line. Moreover, the resonance and forbidden lines of F VIII are close to the $3s \rightarrow 2p$ transitions in Fe XVII and may further alter the inferred apparent Fe XVII line ratios, particularly in spectrometers with moderate spectral resolution. The enhanced emission of line $3C$ can thus serve as a new spectral diagnostic for the detection of fluorine in astrophysical plasmas.

Key words: atomic processes – line: formation – stars: coronae – Sun: X-rays, gamma rays – X-rays: general

1. Introduction

The difficulty in modeling the spectral emission of Fe XVII, i.e., from neon–like Fe^{16+}, has been well documented during the past 20 years. The problems were highlighted by the first high-resolution spectra observed with the *Chandra X-ray Observatory*, which indicated problems with modeling the emission of the five dominant Fe XVII X-ray lines (Behar et al. 2001; Doron & Behar 2002; Xu et al. 2002; Gu et al. 2004; Gu 2009), i.e., the two $3d \rightarrow 2p$ transitions, which are commonly denoted $3C$ and $3D$ in the notation introduced by Parkinson (1973), and the three $3s \rightarrow 2p$ transitions, which are commonly denoted $3F$, $3G$, and $M2$. Prior to the *Chandra* measurements, discrepancies between the models and solar observations of the Fe XVII spectrum had been attributed to resonance scattering of the most intense of the five x-ray lines, namely line $3C$, which also has the largest oscillator strength among these five lines (Schmelz et al. 1992; Waljeski et al. 1994). However, targeted measurements focused on electron-impact excitation cross-sections and oscillator strengths showed that the discrepancy between the observations and spectral models is reproduced in the laboratory (Brown et al. 1998, 2001, 2006; Beiersdorfer et al. 2002; Bernitt et al. 2012). A limited set of measurements were also presented from low-density plasma sources, specifically from tokamaks, which are magnetically confined plasma devices (Beiersdorfer et al. 2001, 2004a). Results for various ratios of the Fe XVII lines derived from spectra collected at tokamaks were in very good agreement with those from solar and astrophysical observations (Beiersdorfer et al. 2001, 2004a). Importantly, the column densities of these laboratory plasmas were small enough so that resonance scattering could not be invoked to explain the discrepancies with the theoretical models.

In the following, we present measurements of the Fe XVII spectral emission from plasmas that are magnetically confined in the National Spherical Torus Experiment (NSTX). These plasmas are formed from hydrogen (deuterium) gas. Ions from other elements—notably carbon and oxygen, and to a lesser degree iron and other constituents of stainless steel—can be present in trace amounts, which vary from discharge to discharge.

NSTX is a so-called spherical torus (Ono et al. 2003; Synakowski et al. 2003; Sabbagh et al. 2013). This is a device similar to a tokamak, except that the minor radius of the torus is greatly increased relative to its major radius. This geometry makes the temperature and density profiles flat in the core, eliminating the central gradients ubiquitous in tokamaks. Reduced gradients diminish plasma effects that might lead to enhanced indirect excitation processes, such as inner-shell ionization and radiative recombination (Beiersdorfer et al. 1990), which can affect the Fe XVII line ratios. The present measurements are thus from plasmas with improved spatial uniformity, extending the previous set of plasma measurements that utilized tokamaks. Our results from typical NSTX plasmas reproduce the Fe XVII line ratios seen in astrophysical observations.

We also report spectra obtained from plasmas that show an apparent enhancement of the $3C$ line. We show that this enhancement is an artifact of line $3C$ blending with the Lyα lines of F IX. Such an enhancement serves as a new diagnostic for the detection of fluorine in astrophysical plasmas.

Although fluorine does not have a high solar abundance, it has been observed in various astrophysical objects, including in interstellar gas (Jorissen et al. 1992; Liu 1998; Federman et al. 2005; Werner et al. 2005; Asplund et al. 2009). The detection of the lesser metals has important implications for nuclear synthesis models. Moreover, their emission spectra may compromise the analysis of astrophysical data if they are not taken into account. For example, the K-shell emission of highly charged potassium has been used to explain (Carlson et al. 2015; Jeltema & Profumo 2015) what otherwise may be an X-ray signature of sterile neutrinos in the spectra of galaxies and galaxy clusters (Boyarsky et al. 2014, 2015; Markevitch et al. 2014; Bulbul et al. 2014, 2016). Indeed, *Hitomi* has recently reported weak X-ray features from hydrogen–like and helium–like potassium in its relatively brief

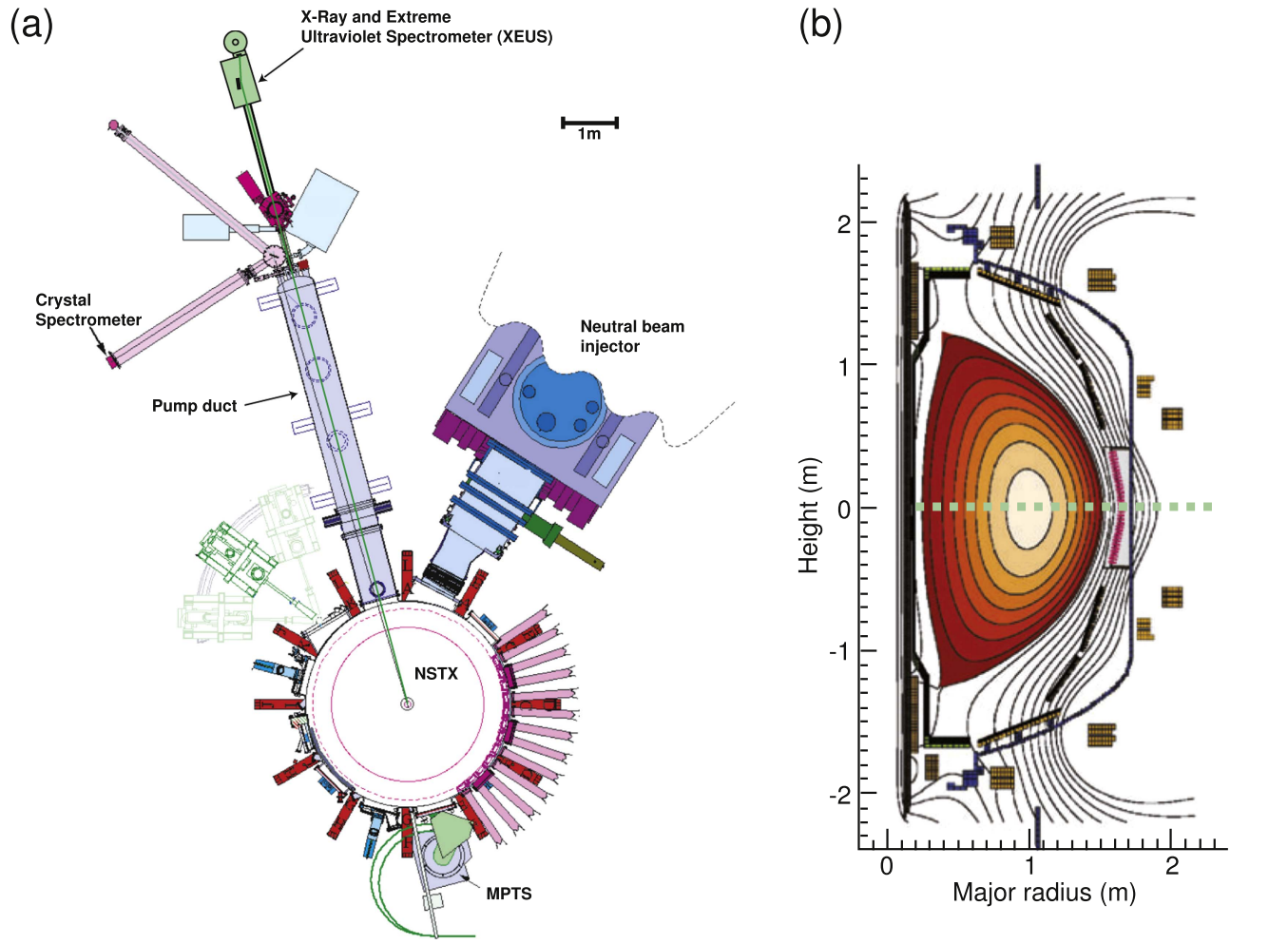

Figure 1. Location of the XEUS instrument on NSTX. (a) The horizontal view showing XEUS at the end of the NSTX pump duct, as well as the location of the neutral beam injector and the multi-point Thomson scattering system (MPTS). (b) The vertical view showing typical surfaces of constant magnetic flux for an applied toroidal field of 0.3 T, as well as the sightline of XEUS (green dashed trace).

observation of the Perseus Cluster (Aharonian et al. 2017). If potassium can be observed in X-ray spectra, then it may be possible to detect the X-ray signature of fluorine. The solar abundance of fluorine is about $1/3$ that of potassium, but its abundance can reach 30–250× the solar value near objects that are believed to synthesize this element (Jorissen et al. 1992; Werner et al. 2005, 2015, 2016). Moreover, its X-ray excitation cross-sections are about an order of magnitude larger than those of potassium.

2. Experiment

The measurements presented in this paper were performed using the X-ray and Extreme Ultraviolet Spectrometer (XEUS) on the NSTX device at Princeton. This instrument is a medium-resolution grating spectrometer, with a resolving power of $\lambda/\Delta\lambda \approx 120$ at 15 Å. A description of the instrument is given by Beiersdorfer et al. (2006, 2008). It is similar to an instrument used on the Livermore EBIT-I electron beam ion trap for measurements of the iron L-shell and M-shell emission lines (Utter et al. 1999; Lepson et al. 2008, 2010) and on the Alcator tokamak for impurity transport measurements (Reinke et al. 2010).

The instrument was mounted in the horizontal midplane of NSTX, as illustrated in Figure 1(a). An entrance slit of 100 μm width determined the grasp and spectral resolution of the instrument. Its resolving power is comparable to that of previous tokamak observations (Phillips et al. 1997; Beiersdorfer et al. 2001, 2004a), all of which, however, had utilized crystal spectrometers.

Depending on the type of camera used to record the spectra, a temporal resolution of about 3 ms can be obtained (Lepson et al. 2012; Weller et al. 2016). For our measurements, we utilized a liquid nitrogen cooled charged couple device (CCD) camera with 1024×1024 pixels, each of which are 25 μm × 25 μm wide. We used the slowest possible readout time in order to obtain the best signal fidelity. In this case, the readout time is about 1 minute. This is too slow to follow the time dynamics of the plasma discharge. Consequently, we installed a shutter mechanism that ensures that data are only collected between about 80 and 240 ms of the discharge when the plasma conditions are reasonably constant.

NSTX plasmas are characterized by a very low aspect ratio R/a, where R is the major radius of the plasma, and a is the minor radius (Synakowski et al. 2003; Kaye et al. 2005; Sabbagh et al. 2013). This is illustrated in Figure 1(b). For

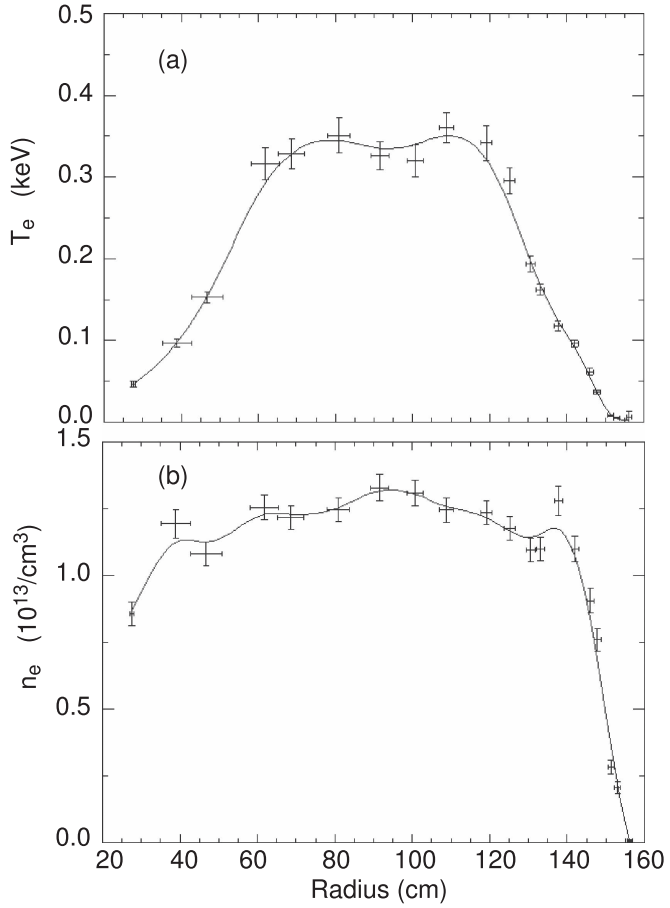

Figure 2. Radial profiles of (a) the electron temperature and (b) the electron density measured with Thomson scattering at $t = 160$ ms for the "cold" NSTX discharge 114478.

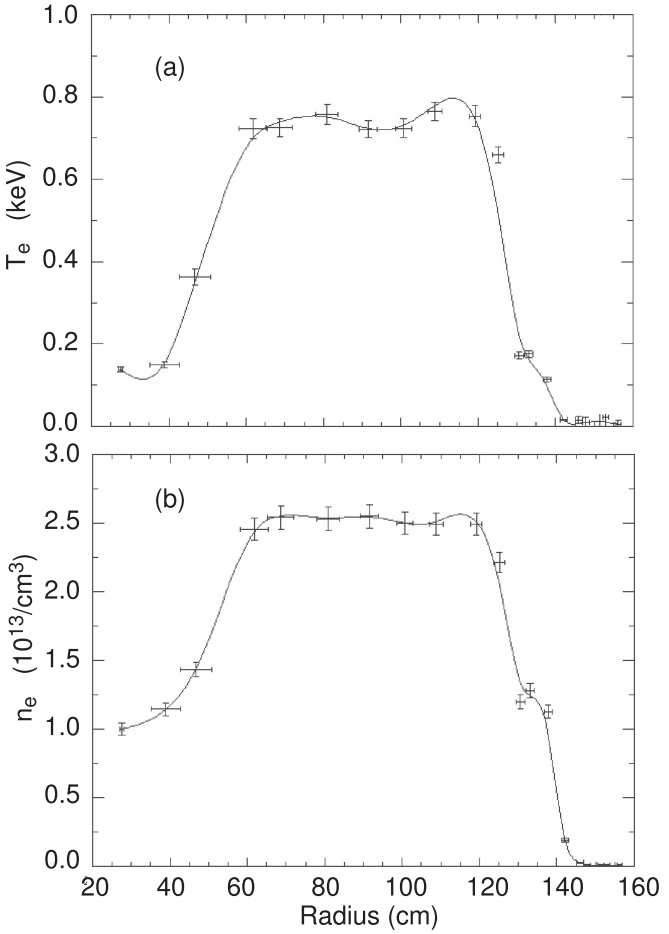

Figure 3. Radial profiles of (a) the electron temperature and (b) the electron density measured with Thomson scattering at $t = 160$ ms for the "hot" NSTX discharge 114459 heated with 6 MW of neutral beam injection.

spectroscopy, this magnetic field configuration has the advantage that temperature and density gradients are minimized, and a large part of the core plasma has the same temperature and density. The temperature and density profiles of interest to our measurements are shown in Figures 2 and 3. As seen from these figures, the electron density is less than about 2.5×10^{13} cm^{-3}, and the profile is essentially flat within most of the central plasma region (60–110 cm). The central temperature is about 350 eV in Figure 2 and about 750 eV in Figure 3. The electron temperature profile is also flat for the inner 60 cm of the plasma core. The flat profiles in NSTX contrast with the parabolic profiles in the tokamak plasmas previously reported for measurements of the Fe XVII lines (Beiersdorfer et al. 2004a), and they reduce the effects caused by gradients, including particle transport.

The difference in the temperature (and density) arises from the amount of heating of the plasma. In both cases, heating is achieved by the plasma current (ohmic heating) and by the injection of an energetic neutral beam (cf. Figure 1). The lower temperature is achieved when the plasma is predominantly ohmically heated. The higher temperature (and density) is attained by elevated neutral beam heating (up to 6 MW).

In Figure 4, we show the measured spectra during the colder and hotter discharges associated with Figures 2 and 3. The spectral region ranges from 6 to 44 Å and is dominated by the strong emission of the $2p \rightarrow 1s$ Lyα lines of C VI and O VIII. The spectral region also contains weak K-shell emission of C V and O VII. The cooler spectrum (Figure 4(a)) shows the L-shell X-ray emission of Fe XVII, and to a smaller extent, the L-shell X-ray emission of Ni XIX. The hotter spectrum (Figure 4(b)) shows additional L-shell X-ray emission of higher charge states of iron. A more detailed view of the spectral region containing the L-shell X-ray emission of iron and nickel is provided in Figure 5. As we have noted before, these elements (C, O, Fe, and Ni) were indigenous impurities of NSTX's hydrogen plasma, and these discharges exhibited no evidence for other impurities, such as fluorine.

In order to understand the spectral emission between 8 and 18 Å, we have produced a collisional-radiative spectral model with data from the Flexible Atomic Code (FAC; Gu 2008). The model assumes that line formation is solely from electron-impact excitation. However, it allows for collisional redistribution of the excited levels, which plays a role at the densities of our plasmas. The model includes the emission from O VIII, the emission from Fe XVII to Fe XXIV, and the emission from Ni XIX, and makes no assumptions on their relative abundances. Individual spectral components included in the model are shown in Figure 6. This figure also shows a fit of the "hot" NSTX spectrum that is based on our model. As a result of this fit, we were able to assign additional identifications of various spectral features.

The fit shown in Figure 6 allows us to identify lines that are significantly blended. For a further analysis, it is very important to note that line $3D$ is blended with the Lyγ line of O VIII. By contrast, lines $3C$ and $3F$ are not significantly blended.

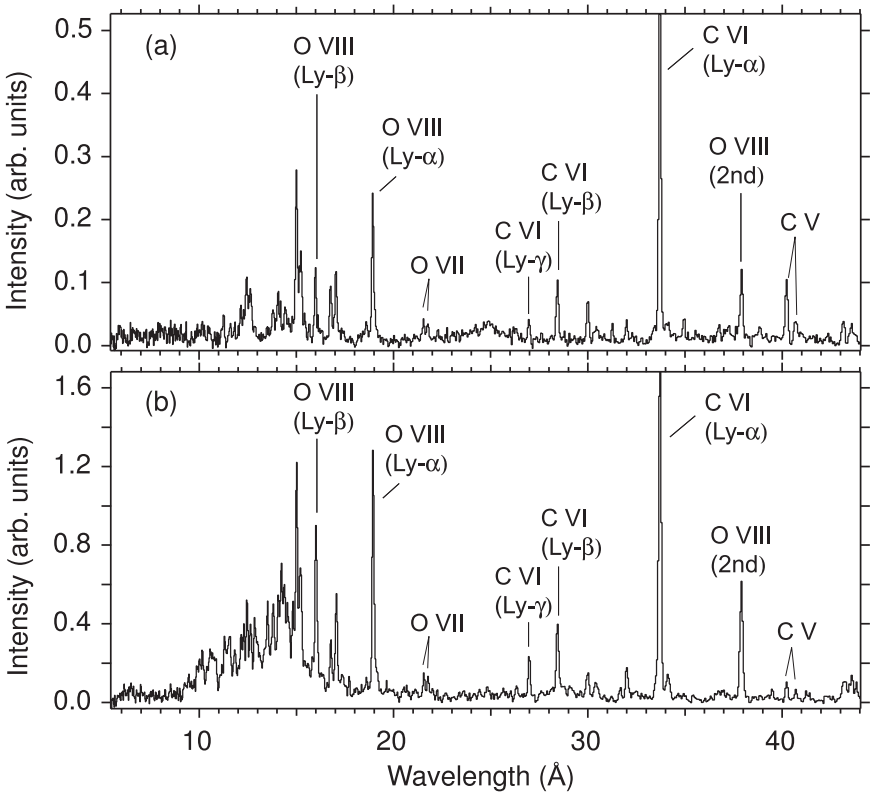

Figure 4. Spectral emission observed with XEUS during the (a) "cold" and (b) "hot" NSTX discharges associated with Figures 2 and 3, respectively. Lyα, Lyβ, and Lyγ denote the $2p \rightarrow 1s$, $3p \rightarrow 1s$, and $4p \rightarrow 1s$ transitions in hydrogen–like ions, respectively. The L-shell emission feature of iron and nickel are located in the 9–18 Å region. This region is shown in detail in Figure 5.

Moreover, while the Fe XVII lines 3*G* and *M*2 are blended with each other, they do not significantly blend with any other emission features. This means that there is a much larger uncertainty in determining the intensity of line 3*D* than of any of the other Fe XVII lines, as oxygen is generally always present in the plasma. In the following, we therefore only concentrate on the emission of lines 3*C*, 3*F*, 3*G*, and *M*2.

Although the presence of O VIII lines is a nuisance for determining the intensity of line 3*D*, it provides a way for calibrating the relative intensity response of XEUS in the 15 to 20 Å region (cf. Beiersdorfer et al. 2004b), which is the region containing the O VIII Lyα, Lyβ, Lyγ, and Lyδ lines (cf. Figures 5 and 6). Being produced by a hydrogen–like ion (i.e., an ion with a single electron), the Lyman series emission can be modeled relatively reliably. We have used a FAC-based collisional-radiative model to predict the O VIII emission at several electron temperatures, two extremes of which bracket the range of temperatures in our NSTX plasmas are shown in Figure 7.

We compare our predictions to the measured intensities of the four Lyman series lines we can resolve in our spectra. Here, we are helped by the fact that there are NSTX discharges with little intrinsic iron and thus only small amounts of iron emission, as illustrated in Figure 8. The intensity of the oxygen Lyman lines can be reliably determined from such spectra and at a reasonably well-defined electron temperature (about 500 eV).

The experimental values of the intensity of the Lyman lines of O VIII relative to that of Lyα are shown in Figure 7 for a comparison with the calculated values. Clearly, the higher series Lyman lines are observed to be stronger than predicted, which is the result of the enhanced reflectivity of the grating for wavelengths near 15 Å, corresponding to the fact that the blaze angle has been optimized for 15 Å (Beiersdorfer et al. 2006). From this comparison, we can derive the relative responsivity curve for XEUS, as shown in Figure 7(b), for the wavelength region of the Fe XVII lines. The three curves shown in the figure illustrate that there is only a slight dependence on the temperature at which the O VIII lines were measured.

3. Results and Comparison with Solar and Astrophysical Observations and Spectral Models

The relative line intensities we infer from the "hot" and "cold" NSTX plasmas shown in the previous section are listed in Table 1. These ratios have been adjusted for the instrumental responsivity. The uncertainties for the "hot" case are significantly larger than for the "cold" case mainly because the uncertainty in determining the individual line intensities, especially that of line 3*C*, is higher as a result of the higher density of the spectral lines and the possibility of additional line blending.

In Figures 9 and 10, we graphically compare our NSTX values with those measured earlier in the Princeton Large Torus tokamak (PLT; Beiersdorfer et al. 2004a), as well as to those observed from the Sun (Parkinson 1973, 1975; Hutcheon et al. 1976; McKenzie et al. 1980; Rugge & McKenzie 1985), the stars Capella (Brinkman et al. 2000; Canizares et al. 2000; Behar et al. 2001; Mewe et al. 2001), Procyon (Raassen et al. 2002), II Pegasi (Huenemoerder et al. 2001), α Centauri (both K1V and G2V; Raassen et al. 2003), and YY Gemini (Stelzer et al. 2002), as well as the galaxy NGC 4636 (Xu et al. 2002). The new NSTX values agree well with the older

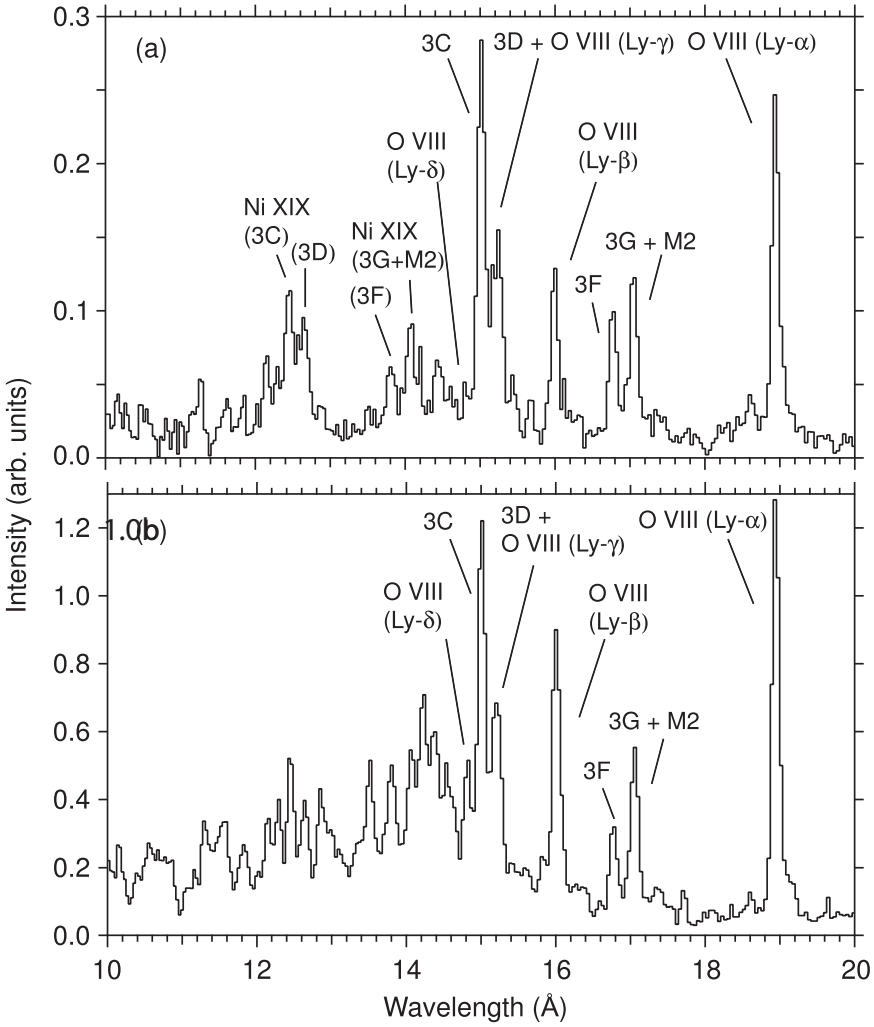

Figure 5. Expanded view of the $n = 3 \rightarrow n = 2$ emission of the iron L-shell emission shown in Figure 4: (a) "cold" and (b) "hot" discharge. The neon–like Fe XVII lines are labeled in the standard notation, where $3C$, $3D$, $3F$, and $3G$ denote the electric dipole transitions from upper levels $1s^2 2s^2 2p^5_{1/2} 3d_{3/2}\ ^1P_1$, $1s^2 2s^2 2p^5_{3/2} 3d_{5/2}\ ^3D_1$, $1s^2 2s^2 2p^5_{1/2} 3s_{1/2}\ ^1P_1$, and $1s^2 2s^2 2p^5_{3/2} 3s_{1/2}\ ^3P_1$, respectively, to the $1s^2 2s^2 2p^6\ ^1S_0$ ground level. $M2$ denotes the magnetic quadrupole transition $2p^5_{3/2} 3s_{1/2}\ ^3P_2 \rightarrow 2p^6\ ^1S_0$. The neon–like Ni XIX lines discernable in (a) are labeled similarly, except that the line designation is in parentheses. Unlabeled features are from the charge states of iron higher than the neon–like (cf. Figure 6).

values from PLT. This agreement indicates that indirect excitation processes (Beiersdorfer et al. 1990) expedited by temperature or density gradients in the older PLT plasmas were not important line formation mechanisms for the Fe XVII lines of interest.

Unlike the disagreement with spectral modeling found by Beiersdorfer et al. (2004a), there is a good agreement with the ratios given by the recent spectral modeling values produced by the AtomDB project V3.0.7 (Smith et al. 2001; Foster et al. 2013). This comparison is illustrated in Figures 9 and 10, where we have plotted the AtomDB modeling ratios calculated at the temperature of maximum emission for Fe XVII (543 eV). Here, we also plot the predictions from Doron & Behar (2002) using their complete, "three-ion model" for two electron temperatures (400 and 600 eV) that bracket the temperature of maximum emission. These and similar calculations by Gu (2003) predict ratios smaller than those measured or observed, on average. The three-ion model includes indirect line formation processes, such as inner-shell ionization, radiative and dielectronic capture, and resonance excitation, which have been shown, in experiments using an electron beam ion trap (Beiersdorfer et al. 1990), to be important for neon–like ions.

It is interesting to note that one of the new NSTX values for the relative intensity of line $3F$ is considerably higher than the AtomDB value. It is also higher than any of the previously measured or observed values. This value comes from the "cold" plasma case, in which the temperature does not exceed 300 eV. This provides a hint that this line ratio may be temperature dependent, as implied by the calculations by Doron & Behar (2002) and Gu (2003). Evidently, more data are needed to confirm this hint.

4. Strong Apparent Enhancement of Line $3C$

Much of the original discrepancy between theory and observation, and between theory and laboratory measurement, could be accounted for with line $3C$ being weaker than modeled (Schmelz et al. 1992; Waljeski et al. 1994; Behar et al. 2001; Beiersdorfer et al. 2001, 2004a; Gu 2009). In fact, measurements of its electron-impact excitation cross-sections showed that they are smaller than originally calculated by theoretical models for all relevant electron energies (Brown

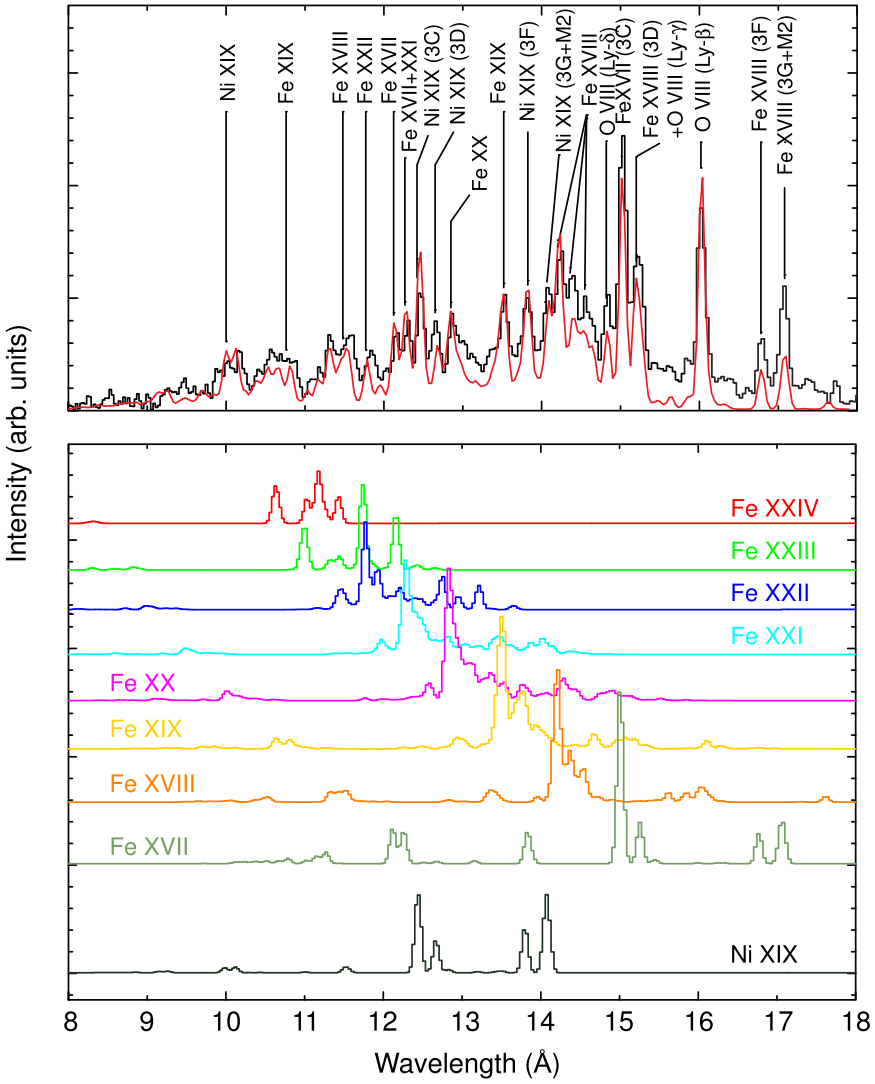

Figure 6. Fit of the "hot" spectral emission observed in the 8–18 Å region using an emission model constructed with the FAC. Contributions from Fe XVII through Fe XXIV, as well as from Ni XIX (not to scale), are shown in the bottom panel. The emission from the Lyman lines of O VIII are also included in the fit.

et al. 2006). It was, therefore, surprising when our experiment on NSTX measured Fe XVII spectra, which appeared to show a greatly enhanced intensity of line 3*C* relative to the other X-ray lines in the Fe XVII spectrum.

The strong apparent intensity enhancement of line 3*C* was observed in multiple NSTX discharges during the neutral beam heating phase. It was absent during the ohmic heating phase before the neutral beam injection and in shots that were only ohmically heated. However, the apparent enhancement was observed only over a time period of a few days, and then was no longer measured under any plasma condition.

The strong apparent enhancement of line 3*C* during the neutral beam heating compared to its intensity during ohmic heating is illustrated in Figure 11. In this figure, line 3*C* appears to double in intensity compared to the other four Fe XVII lines. The apparent intensity ratio of line 3*C* to line 3*D* rises even more dramatically—from about 2.4 in the ohmic case to at least 6.2 in the neutral beam heated discharge. The latter ratio would be even larger and approach infinity if we subtracted away the contribution from the O VIII Lyγ line, as doing so leaves essentially no flux for line 3*D*. By contrast, the other Fe XVII lines do not seem to vanish. However, the apparent intensity of

Table 1
Measured Intensities of $3s \rightarrow 2p$ Transitions Relative to that of the $3d \rightarrow 2p$ Transition 3*C* in Fe XVII

Temperature	I_{3F}/I_{3C}	$I_{3F+3G+M2}/I_{3C}$
"cold"	0.96 ± 0.10	2.36 ± 0.23
"hot"	0.77 ± 0.18	2.43 ± 0.50

the blend of line 3*G* and *M*2 relative to that of line 3*C* seems to diminish more than the apparent intensity of line 3*F*. In fact, in some NSTX discharges, we have measured the apparent blend of 3*G* and *M*2 to be even smaller (by about a factor of two) than what is shown in Figure 11.

The spectrum shown in Figure 11 is thus highly unusual, as it seems to show a greatly enhanced intensity of line 3*C*, while the intensity of line 3*D* appears to vanish, and the intensity of line 3*F* seems to dominate over the intensity of the blend of lines 3*G* and *M*2. No such unusual intensity ratios had been observed before in an Fe XVII X-ray spectrum. Moreover, there are no known excitation conditions that could produce such skewed spectral intensities. Even charge exchange

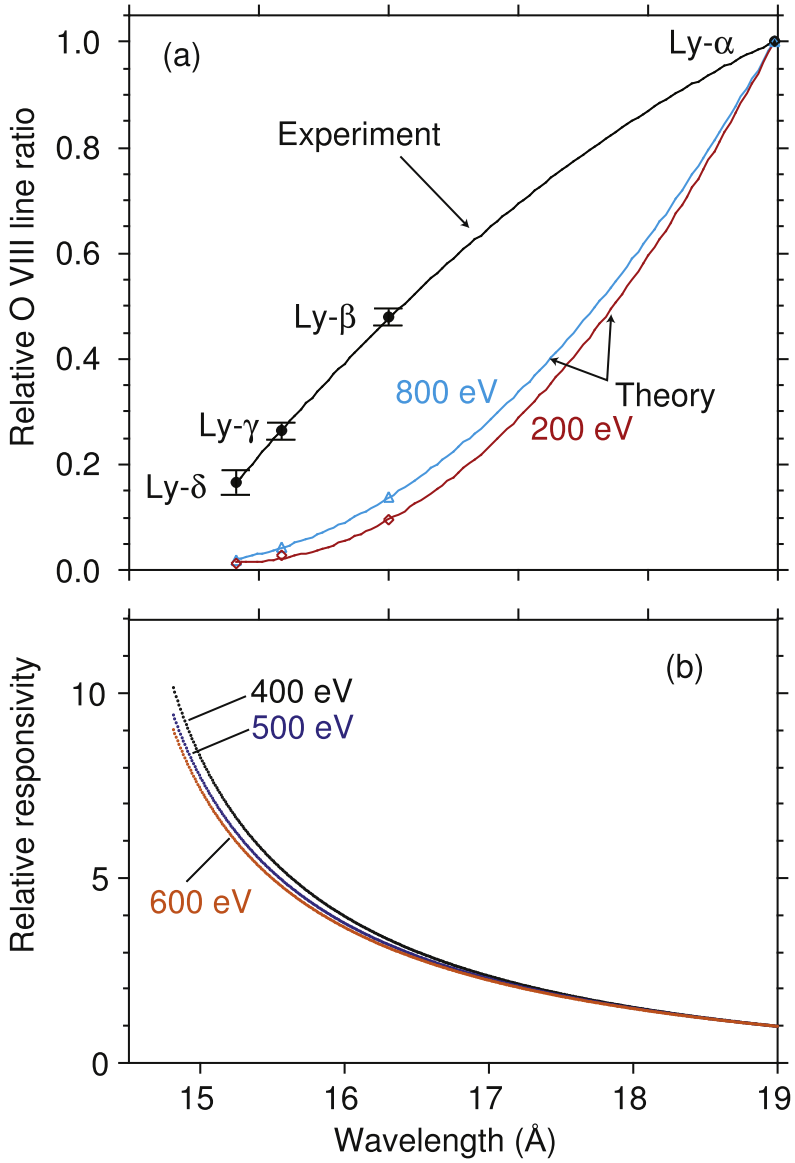

Figure 7. Responsivity determination of XEUS: (a) the experimentally observed O VIII line intensities compared to theoretical predictions from FAC for two extreme temperatures bracketing NSTX plasma temperatures. (b) the relative responsivity of XEUS inferred from (a) for calculated values at 400, 500, and 600 eV. Experimental and theoretical data are fitted by the traces shown in order to enable interpolation of the responsivity at wavelengths between 15 and 19 Å.

recombination, which is known to produce X-ray spectra that differ greatly from those observed in hot, collisional plasmas (Beiersdorfer et al. 2003, 2005; Wargelin et al. 2005, 2008; Leutenegger et al. 2010; Betancourt-Martinez et al. 2014; Ali et al. 2016), does not appear to produce such unusual L-shell X-ray line patterns (Beiersdorfer et al. 2008). The cause for such an unusual line emission pattern must therefore be unrelated to unusual excitation conditions.

We noticed early on that there was an almost imperceptible wavelength shift affecting the apparent Fe XVII lines. However, a shift in itself is not unusual because neutral beam injection may induce bulk plasma motion, which in turn causes the lines to be Doppler shifted. Moreover, electromagnetic pulses affecting the readout electronics and/or mechanical stresses during the plasma discharge, as well as thermal expansion and contraction affecting the spectrometer and camera assembly, have occasionally displaced spectral lines from their otherwise fixed position.

What is more telling than a slight wavelength shift is the addition of a new line in between the apparent positions of the three $3s \rightarrow 2p$ lines $3F$, $3G$, and $M2$ in Fe XVII. The new line could not be attributed to noise or spurious hard X-rays, which may affect the spectra, as the feature was reproducibly visible in all the discharges that exhibited the strong apparent enhancement of line $3C$. Summing the spectra from three neutral beam heated discharges (shots 114465, 114473, and 114475) provided more than enough statistics for a good signal-to-noise ratio to reveal three additional small lines between 12 and 13 Å, which form a pattern in intensity and spectral position that is reminiscent of the Lyman series of O VIII lines between 15 and 16 Å, as illustrated in Figure 8. This suggests that those three lines are the Lyβ, Lyγ, and Lyδ

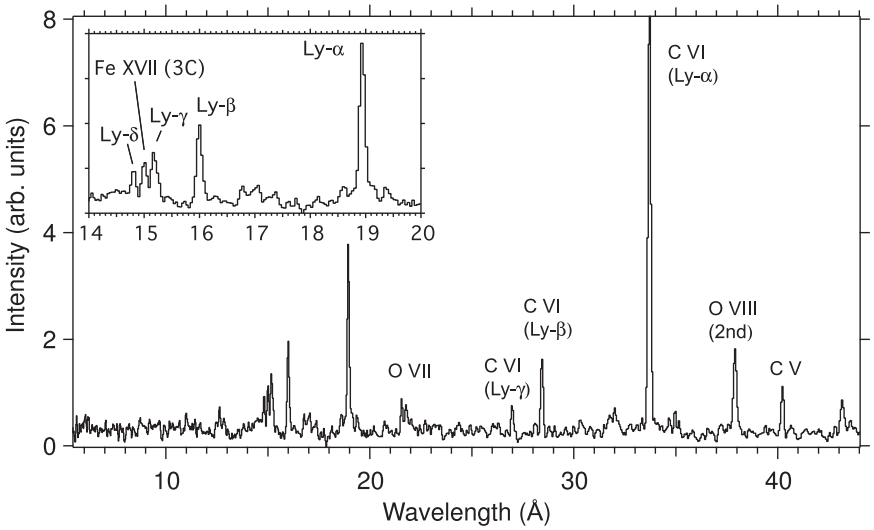

Figure 8. Spectral emission observed with XEUS in the near-absence of L-shell iron lines.

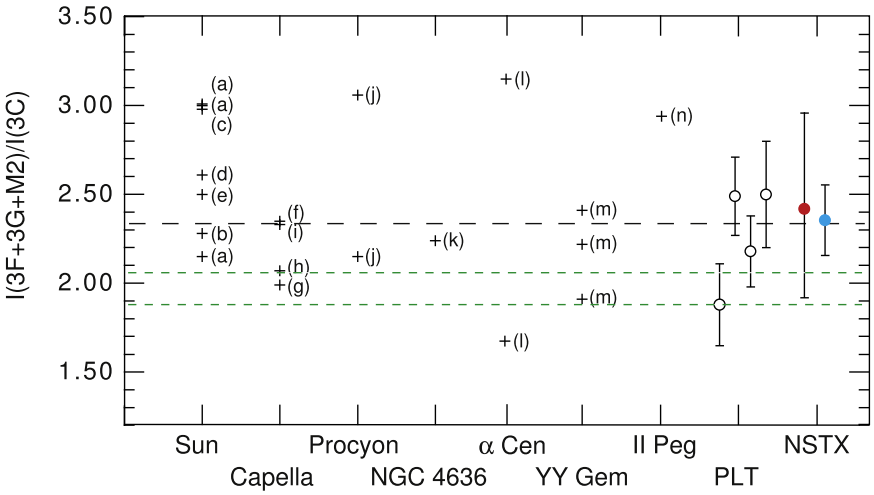

Figure 9. Comparison of the newly measured NSTX $I_{3F+3G+M2}/I_{3C}$ ratios with those measured on the PLT tokamak, as well as with those from solar and astrophysical observations. The legend denotes: (a) Hutcheon et al. (1976), (b) Parkinson (1973), (c) McKenzie et al. (1980), (d) Parkinson (1975), (e) Rugge & McKenzie (1985; average of many values), (f) Behar et al. (2001), (g) Brinkman et al. (2000), (h) Mewe et al. (2001), (i) Canizares et al. (2000), (j) Raassen et al. (2002), (k) Xu et al. (2002), (l) Raassen et al. (2003), (m) Stelzer et al. (2002), and (n) Huenemoerder et al. (2001). Open circles represent measurements on the PLT tokamak (Beiersdorfer et al. 2004a). The datum in blue is from the "cold" discharge (Figure 2); the one in red is from the "hot" discharge (Figure 3). The black, long-dashed horizontal line represents the value given by the AtomDB V3.0.7 spectral model at 543 eV (Foster et al. 2013); the two green, short-dashed lines represent the predictions from Doron & Behar (2002) using their complete, three-ion model for 400 eV (upper trace) and 600 eV (lower trace).

lines of F IX, as illustrated in Figure 12. The strongest of the F IX lines (i.e., Lyα) must then be what appears to be line 3*C* of Fe XVII. In fact, the predicted position of the F IX Lyα line is 14.9841 Å (Garcia & Mack 1965), while that of line 3*C* is 15.012 Å (Beiersdorfer & Wargelin 1994; Brown et al. 1998), as detailed in Table 2. This means that the 2 lines are separated by $\Delta\lambda$: λ of only one part in 538. This is smaller than the 1 part in 378 separation of lines 3*G* and *M*2, which are always seen as blended in our measurements.

The wavelength values listed in Table 2 give additional near coincidences between fluorine and iron lines. The resonance line of F VIII, labeled *w* in common notation, has a wavelength of 16.806 Å, while that of line 3*F* is 16.777 Å. The wavelength of the forbidden F VIII line, labeled *z*, has a wavelength of 17.153 Å, while that of line *M*2 is 17.097 Å, which is a separation of 1 part in 300 (and a separation of about 1 part in 200 from the average position of lines 3*G* and *M*2).

The F VIII intercombination line *y* is predicted to be situated at 16.950 Å (Drake 1988) and thus matches very well with the position of the newly seen line in between the position of lines 3*F* and the blend of 3*G* and *M*2. Line *y* is weak in low-density plasmas; however, at the density of the NSTX plasmas, the forbidden line *z* is collisionally quenched and its flux is transferred to that of line *y*. This means that given the background level, no discernable flux from *y* would have been observed between the locations of the two $3s \rightarrow 2p$ Fe XVII features if the density of NSTX was lower by about a factor of 10 (Mauche et al. 2005; Porquet et al. 2010). Instead, line *z* would have been stronger and would mimick the combined intensity of lines 3*G* and *M*2. In other words, at densities below about 10^{12} cm^{-1}, it would have been much more

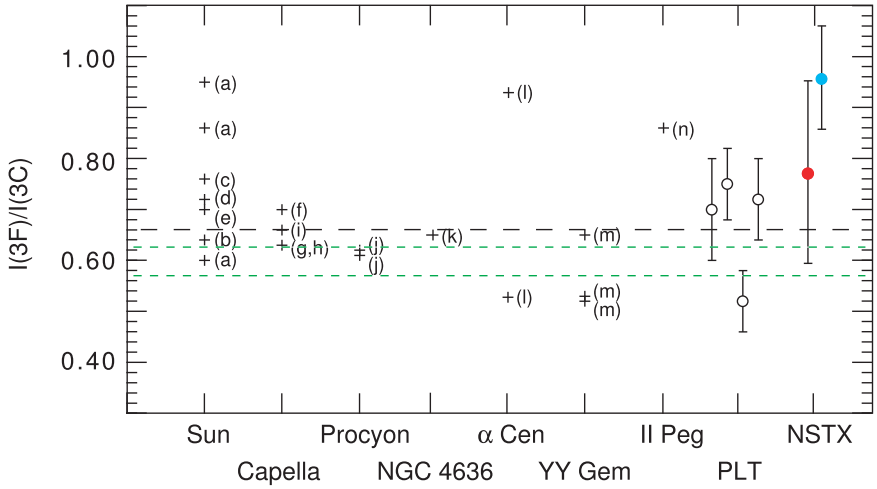

Figure 10. Comparison of the newly measured NSTX I_{3F}/I_{3C} ratios with those measured on the PLT tokamak, as well as with those from solar and astrophysical observations. The legend denotes: (a) Hutcheon et al. (1976), (b) Parkinson (1973), (c) McKenzie et al. (1980), (d) Parkinson (1975), (e) Rugge & McKenzie (1985; average of many values), (f) Behar et al. (2001), (g) Brinkman et al. (2000), (h) Mewe et al. (2001), (i) Canizares et al. (2000), (j) Raassen et al. (2002), (k) Xu et al. (2002); (l) Raassen et al. (2003), (m) Stelzer et al. (2002), and (n) Huenemoerder et al. (2001). Open circles represent measurements on the PLT tokamak (Beiersdorfer et al. 2004a). The datum in blue is from the "cold" discharge (Figure 2); the one in red is from the "hot" discharge (Figure 3). The black, long-dashed horizontal line represents the value given by the AtomDB V3.0.7 spectral model at 543 eV (Foster et al. 2013); the two green, short-dashed lines represent the predictions from Doron & Behar (2002) using their complete, three-ion model for 400 eV (upper trace) and 600 eV (lower trace).

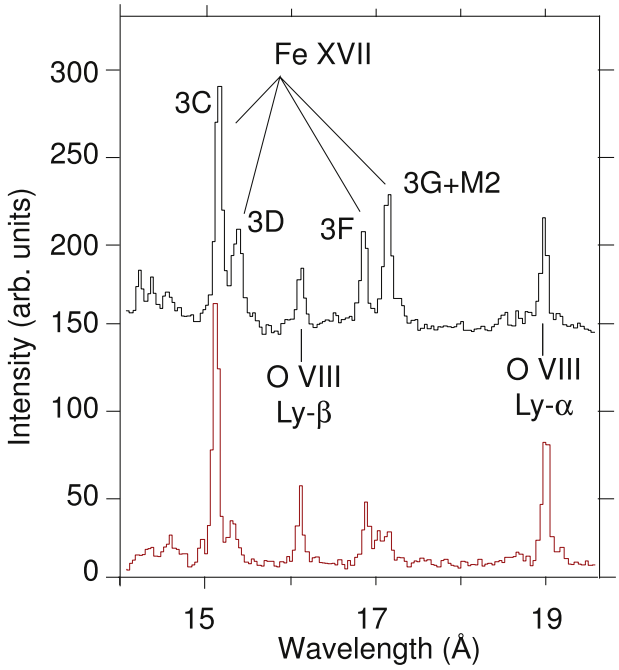

Figure 11. Spectral emission measured in neutral beam heated NSTX discharges, showing an apparent enhancement of line 3*C* (red, bottom trace). For comparison, the Fe XVII X-ray spectrum measured during ohmic heating (black, top trace) does not show an enhancement.

difficult to identify the X-ray emission of fluorine as the cause for the enhanced apparent intensity of line 3*C*.

A summary of the X-ray lines detected from F VIII and F IX is also provided in Figure 12, where we have marked the location of the fluorine lines we have identified. In addition to those lines already mentioned, we have also identified the $1s_{1/2}3p_{3/2} \rightarrow 1s^2$ resonance line in F VIII.

Fluorine is not an indigenous trace element in NSTX plasmas. It was only seen during a few days of experiments and only during the neutral beam heating phase. The source of the fluorine remains unknown. Of course, smaller amounts of fluorine would produce weaker lines that blend with the Fe XVII lines and therefore may be detectable only via a weak enhancement of line 3*C*.

5. Summary and Discussion

We have presented spectra of the Fe XVII emission from magnetically confined plasmas at densities comparable to those found in solar flares. Unlike the plasmas of earlier

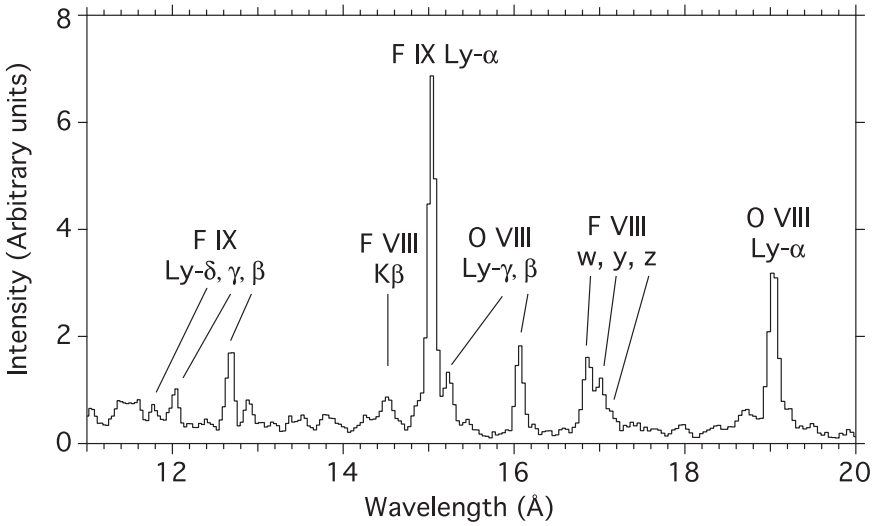

Figure 12. Spectral emission observed with XEUS during neutral beam heated NSTX discharges. Spectra from three discharges have been summed to enhance the signal-to-noise ratio. Lyα, Lyβ, Lyγ, and Lyδ denote the $2p \rightarrow 1s$, $3p \rightarrow 1s$, $4p \rightarrow 1s$, and $5p \rightarrow 1s$ transitions in hydrogen–like F IX, respectively. The resonance, intercombination, and forbidden lines that proceed from upper levels $1s_{1/2}2p_{3/2}\ ^1P_1$, $1s_{1/2}2p_{1/2}\ ^3P_1$, and $1s_{1/2}2s_{1/2}\ ^3S_1$ to the $1s^2\ ^1S_0$ ground level of F VIII are labeled *w*, *y*, and *z*, respectively. Kβ denotes the $1s_{1/2}3p_{3/2}\ ^1P_1 \rightarrow 1s^2\ ^1S_0$ transition in F VIII.

Table 2
Wavelength Comparison of Transitions in Fe XVII, F VIII, and F IX

Label	Ion	Transition	Wavelength (Å)
Lyα	F IX	$2p_{1/2,3/2} \rightarrow 1s_{1/2}$	14.984[a]
3*C*	Fe XVII	$1s^22s^2p^5_{1/2}3d_{3/2} \rightarrow 1s^22s^22p^6$	15.012[b]
w	F VIII	$1s_{1/2}2p_{3/2} \rightarrow 1s^2$	16.806[c]
3*F*	Fe XVII	$1s^22s^2p^5_{1/2}3s_{1/2} \rightarrow 1s^22s^22p^6$	16.777[b]
y	F VIII	$1s_{1/2}2p_{1/2} \rightarrow 1s^2$	16.950[c]
3*G*	Fe XVII	$1s^22s^2p^5_{3/2}3s_{1/2} \rightarrow 1s^22s^22p^6$	17.052[b]
*M*2	Fe XVII	$1s^22s^2p^5_{3/2}3s_{1/2} \rightarrow 1s^22s^22p^6$	17.097[b]
z	F VIII	$1s_{1/2}2s_{1/2} \rightarrow 1s^2$	17.153[c]

Notes.
[a] Wavelength from Garcia & Mack (1965).
[b] Average of measurements from Beiersdorfer & Wargelin (1994) and Brown et al. (1998).
[c] Wavelength from Drake (1988).

measurements (Beiersdorfer et al. 2001, 2004a), the present plasmas have greatly reduced spatial gradients in density and temperature. There is not only an excellent agreement with the spectra from astrophysical observations, but also with earlier plasma measurements, suggesting that gradients do not significantly affect the spectral line intensities. We showed that blending with the F IX emission may dramatically increase the apparent intensity of line 3*C*, while the F VIII X-ray emission affects the apparent intensities of line 3*F* and the blend of lines 3*G* and *M*2.

The astrophysical abundance of fluorine is low—about three dex lower in the Sun than that of Fe (Asplund et al. 2009). To our knowledge, F VIII and F IX X-ray features have not yet been detected in the spectra of the Sun or other stars. However, some stars exhibit fluorine abundances that are orders of magnitude above solar (Werner et al. 2005, 2015, 2016). This, and the fact that the search for the source of fluorine is still ongoing (Federman et al. 2005), suggests that detection in the X-ray range may be possible.

Instruments such as the grating spectrometer aboard the *XMM-Newton X-ray Observatory*, the Low Energy Transmission Grating Spectrometer aboard the *Chandra X-ray Observatory*, or the X-ray microcalorimeter aboard *Hitomi* (Kelley et al. 2016; Hitomi Collaboration et al. 2016) have a resolving power similar to that of our measurements near 15 Å, making it similarly difficult to directly detect the X-ray emission lines of fluorine in the presence of the Fe XVII emission. However, because the emission from F VIII and F IX can skew the spectral pattern of the Fe XVII lines, fluorine can be detected via the intensities of the apparent Fe XVII lines, as we have demonstrated in our NSTX measurements. In particular, any detection of unusually strong emission in line 3*C*, especially relative to line 3*D*, should be taken as an indication of blending with the Lyα line of F IX, thus as a potential detection of fluorine.

This work was supported by the Office of Fusion Energy Sciences as part of the Basic Plasma Science initiative. Work by the Lawrence Livermore National Laboratory was performed under the auspices of the Department of Energy under Contract DE-AC52-07NA27344; work by the Princeton University Plasma Physics Laboratory was performed under the auspices of the Department of Energy under Contract DE-AC02-76CHO3073. The digital data for this paper can be found at http://arks.princeton.edu/ark:/88435/dsp01d504rn98q.

ORCID iDs

P. Beiersdorfer https://orcid.org/0000-0003-0127-599X

References

Aharonian, F. A., Akamatsu, H., Akimoto, F., et al. 2017, ApJL, 837, L15
Ali, R., Beiersdorfer, P., Harris, C. L., & Neill, P. A. 2016, PhRvA, 93, 012711
Asplund, M., Grevesse, N., Sauval, A. J., & Scott, P. 2009, ARA&A, 47, 481
Behar, E., Cottam, J., & Kahn, S. M. 2001, ApJ, 548, 966
Beiersdorfer, P., Behar, E., Boyce, K. R., et al. 2002, ApJL, 576, L169
Beiersdorfer, P., Bitter, M., Marion, M., & Olson, R. E. 2005, PhRvA, 72, 032725

Beiersdorfer, P., Bitter, M., Roquemore, L., Lepson, J. K., & Gu, M.-F. 2006, RScI, 77, 10F306
Beiersdorfer, P., Bitter, M., von Goeler, S., & Hill, K. W. 2004a, ApJ, 610, 616
Beiersdorfer, P., Boyce, K. R., Brown, G. V., et al. 2003, Sci, 300, 1558
Beiersdorfer, P., Lepson, J. K., Bitter, M., Hill, K. W., & Roquemore, L. 2008, RScI, 79, 10E318
Beiersdorfer, P., Magee, E. W., Träbert, E., et al. 2004b, RScI, 75, 3723
Beiersdorfer, P., Osterheld, A. L., Chen, M. H., et al. 1990, PhRvL, 65, 1995
Beiersdorfer, P., Schweikhard, L., Liebisch, P., & Brown, G. V. 2008, ApJ, 672, 726
Beiersdorfer, P., von Goeler, S., Bitter, M., & Thorn, D. B. 2001, PhRvA, 64, 032705
Beiersdorfer, P., & Wargelin, B. J. 1994, RScI, 65, 13
Bernitt, S., Brown, G. V., Rudolph, J. K., et al. 2012, Natur, 492, 225
Betancourt-Martinez, G. L., Beiersdorfer, P., Brown, G. V., et al. 2014, PhRvA, 90, 052723
Boyarsky, A., Franse, J., Iakubovskyi, D., & Ruchayskiy, O. 2015, PhRvL, 115, 161301
Boyarsky, A., Ruchayskiy, O., Iakubovskyi, D., & Franse, J. 2014, PhRvL, 113, 251301
Brinkman, A. C., Gunsing, C. J. T., Kaastra, J. S., et al. 2000, ApJL, 530, L111
Brown, G. V., Beiersdorfer, P., Chen, H., et al. 2006, PhRvL, 96, 253201
Brown, G. V., Beiersdorfer, P., Kahn, S. M., Liedahl, D. A., & Widmann, K. 1998, ApJ, 502, 1015
Brown, G. V., Beiersdorfer, P., & Widmann, K. 2001, PhRvA, 63, 032719
Bulbul, E., Markevitch, M., Foster, A., et al. 2014, ApJ, 789, 13
Bulbul, E., Markevitch, M., Foster, A., et al. 2016, ApJ, 831, 55
Canizares, C. R., Huenemoerder, D. P., Davis, D. S., et al. 2000, ApJL, 539, L41
Carlson, E., Jeltema, T., & Profumo, S. 2015, JCAP, 2, 009
Doron, R., & Behar, E. 2002, ApJ, 574, 518
Drake, G. W. F. 1988, CaJPh, 66, 586
Federman, S. R., Sheffer, Y., Lambert, D. L., & Smith, V. V. 2005, ApJ, 619, 884
Foster, A. R., Ji, L., Yamaguchi, H., Smith, R. K., & Brickhouse, N. S. 2013, in AIP Conf. Ser. 1545, Eighth International Conference on Atomic and Molecular Data and their Applications: ICAMDATA-2012, ed. J. D. Gillaspy, W. L. Wiese, & Y. A. Podpaly (Melville, NY: AIP), 252
Garcia, J. D., & Mack, J. E. 1965, JOSA, 55, 654
Gu, M.-F. 2003, ApJ, 582, 1241
Gu, M. F. 2008, CaJPh, 86, 675
Gu, M. F. 2009, arXiv:0905.0519
Gu, M.-F., Beiersdorfer, P., Brown, G. V., et al. 2004, ApJL, 607, L143
Hitomi Collaboration, Aharonian, F., Akamatsu, H., Akimoto, F., et al. 2016, Natur, 535, 117
Huenemoerder, D. P., Canizares, C. R., & Schulz, N. S. 2001, ApJ, 559, 1135
Hutcheon, R. J., Pye, J. P., & Evans, K. D. 1976, MNRAS, 175, 489
Jeltema, T., & Profumo, S. 2015, MNRAS, 450, 2143
Jorissen, A., Smith, V. V., & Lambert, D. L. 1992, A&A, 261, 164
Kaye, S. M., Bell, M. G., Bell, R. E., et al. 2005, NucFu, 45, S168
Kelley, R. L., Akamatsu, H., Azzarello, P., et al. 2016, Proc. SPIE, 9905, 99050V
Lepson, J., Beiersdorfer, P., Bitter, M., & Kahn, S. M. 2008, CaJPh, 86, 175
Lepson, J., Beiersdorfer, P., Clementson, J., et al. 2010, JPhB, 43, 144018
Lepson, J., Beiersdorfer, P., Clementson, J., et al. 2012, RScI, 83, 10D520
Leutenegger, M. A., Beiersdorfer, P., Brown, G. V., et al. 2010, PhRvL, 105, 063201
Liu, X.-W. 1998, MNRAS, 295, 699
Mauche, C. W., Liedahl, D. A., & Fournier, K. B. 2005, in AIP Conf. Ser. 774, X-ray Diagnostics of Astrophysical Plasmas: Theory, Experiment, and Observation, ed. R. Smith (Melville, NY: AIP), 133
McKenzie, D. L., Landecker, P. B., Broussard, R. M., et al. 1980, ApJ, 241, 409
Mewe, R., Raassen, a. J. J., Drake, J. J., et al. 2001, A&A, 368, 888
Ono, M., Bell, M. G., Bell, R. E., et al. 2003, PPCF, 45, A335
Parkinson, J. H. 1973, A&A, 24, 215
Parkinson, J. H. 1975, SoPh, 42, 183
Phillips, K. J. H., Greer, C. J., Bhatia, A. K., et al. 1997, A&A, 324, 381
Porquet, D., Dubau, J., & Grosso, N. 2010, SSRv, 157, 103
Raassen, A. J. J., Mewe, R., Audard, M., et al. 2002, A&A, 389, 228
Raassen, A. J. J., Ness, J.-U., Mewe, R., et al. 2003, A&A, 400, 671
Reinke, M. L., Beiersdorfer, P., Howard, N. T., et al. 2010, RScI, 81, 10D736
Rugge, H. R., & McKenzie, D. L. 1985, ApJ, 297, 338
Sabbagh, S. A., Ahn, J.-W., Allain, J., et al. 2013, NucFu, 53, 104007
Schmelz, J. Y., Saba, J. L. R., & Strong, K. T. 1992, ApJL, 398, L115
Smith, R. K., Brickhouse, N. S., Liedahl, D. A., & Raymond, J. C. 2001, ApJL, 556, L91
Stelzer, B., Burwitz, V., Audard, M., et al. 2002, A&A, 392, 585
Synakowski, E. J., Bell, M. G., Bell, R. E., et al. 2003, NucFu, 43, 1653
Utter, S. B., Brown, G. V., Beiersdorfer, P., Clothiaux, E. J., & Podder, N. K. 1999, RScI, 70, 284
Waljeski, K., Moses, D., Dere, K. P., et al. 1994, ApJ, 429, 909
Wargelin, B. J., Beiersdorfer, P., & Brown, G. V. 2008, CaJPh, 86, 151
Wargelin, B. J., Beiersdorfer, P., Neill, P. A., Olson, R. E., & Scofield, J. H. 2005, ApJ, 634, 687
Weller, M. E., Beiersdorfer, P., Soukhanovskii, V. A., Magee, E. W., & Scotti, F. 2016, RScI, 87, 11E324
Werner, K., Rauch, T., & Kruk, J. W. 2005, A&A, 433, 641
Werner, K., Rauch, T., & Kruk, J. W. 2015, A&A, 582, A94
Werner, K., Rauch, T., & Kruk, J. W. 2016, A&A, 593, A104
Xu, H., Kahn, S. M., Peterson, J. R., et al. 2002, ApJ, 579, 600